2007

Symmetry breaking in linearly coupled dynamical lattices

G Herring

PG Kevrekidis
University of Massachusetts - Amherst, kevrekid@math.umass.edu

BA Malomed

R Carretero-Gonzalez

DJ Frantzeskakis

Symmetry Breaking in Linearly Coupled Dynamical Lattices

G. Herring and P.G. Kevrekidis
Department of Mathematics and Statistics, University of Massachusetts, Amherst MA 01003-4515, USA

B.A. Malomed
Department of Interdisciplinary Studies, Faculty of Engineering, Tel Aviv University, Tel Aviv 69978, Israel

R. Carretero-González
Nonlinear Dynamical Systems Group, Department of Mathematics and Statistics, and Computational Science Research Center, San Diego State University, San Diego CA, 92182-7720, USA

D.J. Frantzeskakis
Department of Physics, University of Athens, Panepistimiopolis, Zografos, Athens 15784, Greece
(Dated: Submitted to *Phys. Rev.E*, April, 2007.)

We examine one- and two-dimensional (1D and 2D) models of linearly coupled lattices of the discrete-nonlinear-Schrödinger type. Analyzing ground states of the systems with equal powers in the two components, we find a symmetry-breaking phenomenon beyond a critical value of the squared l^2-norm. Asymmetric states, with unequal powers in their components, emerge through a subcritical pitchfork bifurcation, which, for very weakly coupled lattices, changes into a supercritical one. We identify the stability of various solution branches. Dynamical manifestations of the symmetry breaking are studied by simulating the evolution of the unstable branches. The results present the first example of spontaneous symmetry breaking in 2D lattice solitons. This feature has no counterpart in the continuum limit, because of the collapse instability in the latter case.

I. INTRODUCTION

Dynamical lattices and their applications have become an area of increasing interest over the past decade, as shown by a multitude of recent reviews of the topic [1]-[3]. This growth was driven by a wide array of physical realizations, in fields as diverse as light propagation in optical waveguide arrays [4], dynamics of Bose-Einstein condensates (BECs) in periodic potentials (optical lattices) [5], micro-mechanical cantilever arrays [3], models of DNA [6], and others. A key model that has been widely used and analyzed in each of the above areas is the discrete nonlinear Schrödinger (DNLS) equation [2]. In these applications, it emerges either as a tight-binding approximation (as in the case of BECs trapped in optical lattices), or at the level of an envelope-wave expansion of the underlying physical field (such as the electromagnetic field of light in the optical systems).

One aspect of this class of discrete dynamical models which remains perhaps less explored concerns their multi-component generalizations, which are relevant to many fields where dynamical lattices are natural models. For instance, in the case of waveguide arrays, one may consider settings with two orthogonal polarizations of light [7], or two different wavelengths, see e.g., Ref. [8]. Similarly, in the BEC context, one may consider multi-species condensates in the form of mixtures of different hyperfine states in ^{87}Rb [9, 10] and ^{23}Na [11], or mixtures of different atomic species, such as Na–Rb, K–Rb, Cs–Rb, Li–Rb, as well as Li–Cs (see, e.g., Ref. [12] and references therein).

While the above settings are typically modeled by systems of DNLS equations which are coupled by nonlinear terms, such as the ones accounting for the cross-phase modulation in optics, or collisions between atoms belonging to different BEC species, it is also relevant to consider *linearly coupled* DNLS equations (or, in other discrete settings, linearly coupled Ablowitz-Ladik equations [13]). In the optics context, such systems of linearly coupled DNLS equations are relevant to various applications: for example, linear coupling occurs among the two modes inside each waveguide, which may be induced by a twist of the waveguide (for linear polarizations), or by birefringence (for circular polarizations), or in a dual-core structure of the waveguide [8]. On the other hand, in BECs, a linear coupling may be imposed by an external microwave or radio-frequency field, which can drive Rabi [14] or Josephson [15] oscillations between populations of two different states.

In the present work, motivated by the earlier works [16, 17, 18], which studied effects of the linear coupling in various continuum optical models, and also the analysis of the symmetry breaking of discrete two-component solitons in the linearly coupled Ablowitz-Ladik system [13], we consider a system of two DNLS equations coupled *solely* by linear terms. In the optical setting, this would be the above-mentioned discrete analog of a dual-core fiber [16]. Such a model has also been proposed as a means for realization of all-optical switching in ultrashort photonic-crystal couplers [19]. In BECs, it may model the dynamics of two coupled hyperfine states (e.g., of ^{87}Rb), where we imply the use of Feshbach-resonance techniques [20] to nullify the nonlinear interaction between the components (by rendering the respective inter-species scattering length equal to zero). At the same time, two spin states may be linearly coupled due to a

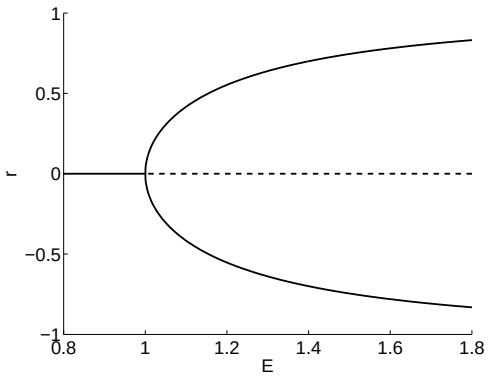

FIG. 1: Bifurcation diagram of solutions for the anti-continuum limit, $\epsilon = 0$; r and E are the asymmetry parameter and the half of the total squared norm, respectively (see the text for the mathematical definitions). The solid and dashed lines show stable and unstable solutions, respectively.

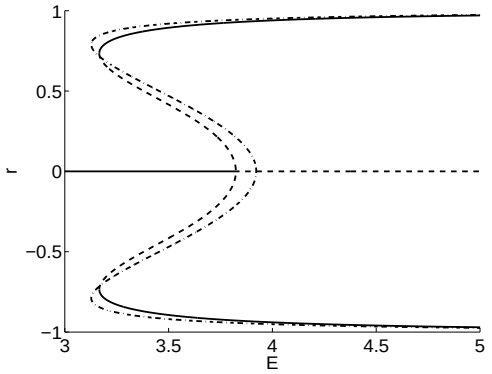

FIG. 2: Bifurcation diagrams for $\epsilon = 1.6$ in the 1D model. The dashed-dotted line indicates solutions found by means of the variational approximation, while solid and dashed lines show, respectively, numerically found stable and unstable steady-state solutions.

resonant spin-flipping radio-frequency field, as mentioned above. In both media (optical and atomic), the relevant model takes the following form:

$$\begin{cases} iU_t = K\epsilon\Delta_2 U + KV + |U|^2 U \\ iV_t = K\epsilon\Delta_2 V + KU + |V|^2 V \end{cases}, \tag{1}$$

where $U = U(\vec{x}, t)$ and $V = V(\vec{x}, t)$ are the wave functions in BEC or electric field envelopes in optics ($\vec{x}$ is realized as a set of discrete coordinates), Δ_2 is the discrete Laplacian, formed by the centered difference in each of the relevant dimensions, K is the strength of the linear coupling between fields U and V, and ϵ determines the couplings between adjacent sites of the lattice. Note that, for convenience, the full coupling constant is defined as $K\epsilon$; this convention will allow us to eliminate K from the analysis presented below.

Our aim is to find and explore in detail the symmetry-breaking bifurcation of the ground-state single-pulse solution of Eqs. (1), similar to the earlier studies performed for continuum models in Refs. [16, 17, 18]. We will address this problem analytically, by means of a variational approximation (VA), and numerically, via computations of the steady-state bifurcations and linear stability, as well as through direct numerical simulations testing the stability or instability of states under consideration. In this way, we obtain a complete bifurcation diagram of the discrete model. A unique advantage of performing this analysis in the discrete setting is that the bifurcation diagram can be produced not only for one-dimensional (1D), but also for two-dimensional (2D) lattices. The latter is impossible in usual continuum models of the cubic-NLS type because of the collapse instability [21]. However, it was demonstrated in Ref. [22] (see also Ref. [2]) that the DNLS with sufficiently weak inter-site coupling [i.e., small coefficient ϵ in Eqs. (1)] gives rise to *stable* discrete 2D solitons. This permits us to construct a bifurcation diagram for the 2D lattice and compare it to the 1D counterpart. To the best of our knowledge, this is the first time that a symmetry-breaking bifurcation is found and analyzed in a 2D model with the cubic nonlinearity.

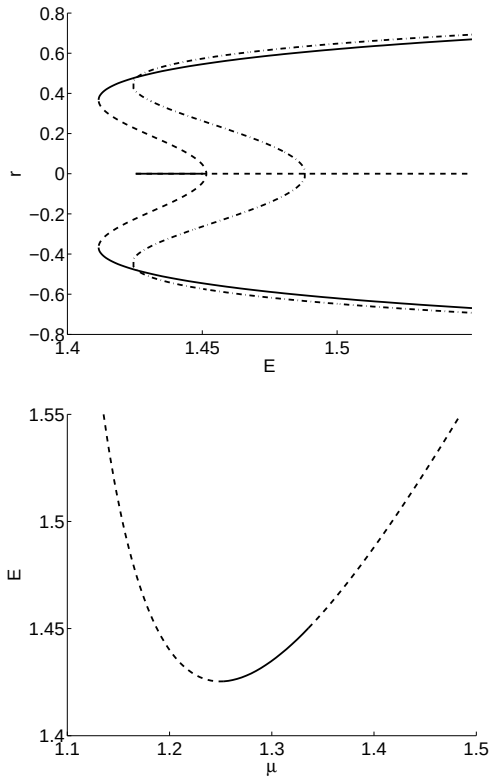

FIG. 3: The top panel shows the bifurcation diagram in the 2D model for $\epsilon = 0.25$, in the same way as the 1D diagram is shown in Fig. 2. The bottom panel displays the dependence of the solution's squared norm, E, upon the chemical potential, μ, for the symmetric solutions. Unlike the 1D case, there are two different symmetric solutions for many values of E, resulting in both stable and unstable solutions for norms below the value at which the symmetric and asymmetric solution branches intersect.

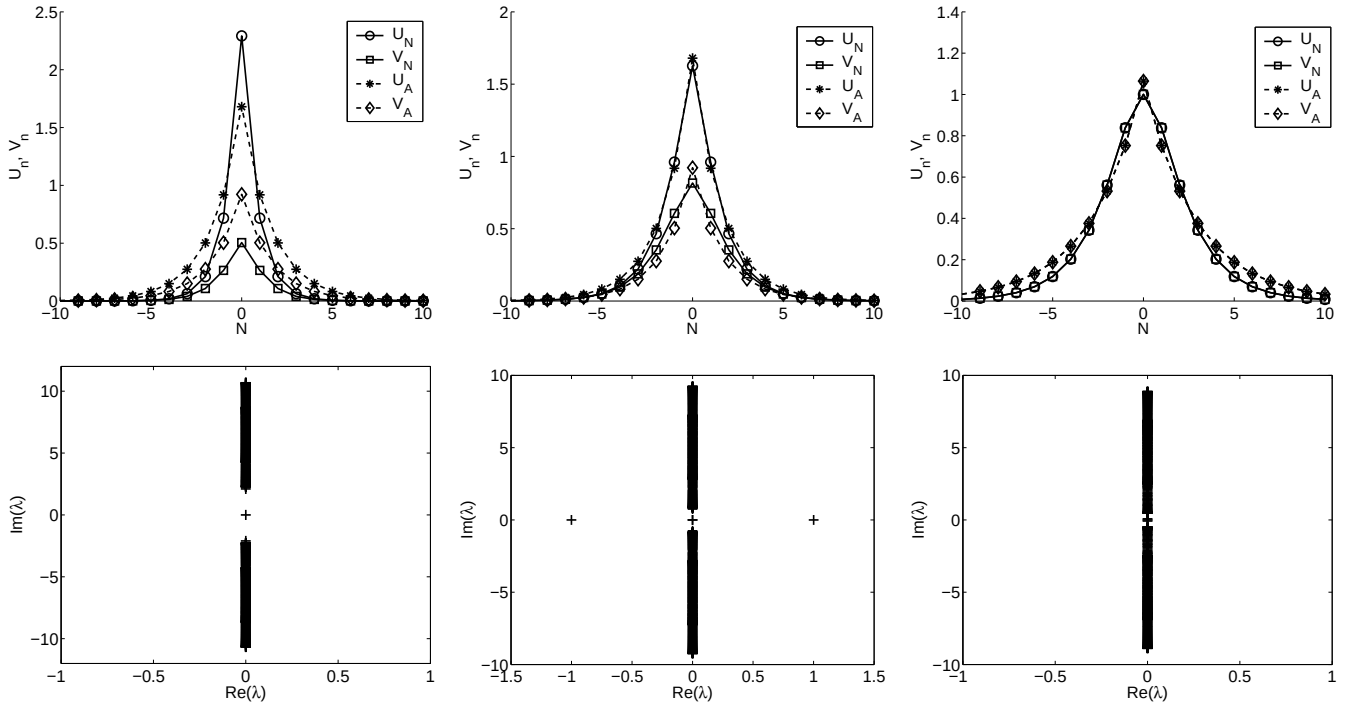

FIG. 4: Plots of solutions from the branch in Fig. 2 for $E = 3.4$. The top-row figures show the solution profiles found by means of the numerical (U_N, V_N) and variational ("analytical", U_A, V_A) methods. The bottom row plots illustrate the stability eigenvalues for the numerical solution. The first column presents a stable stationary asymmetric solution from the outer (upper) branch in Fig. 2, the second column is an unstable asymmetric solution of the inner branch, and the last column is taken from the stable part of the family of symmetric solutions, with $r = 0$.

The paper is structured as follows. In Section 2, we present the model and analytical results, based on the variational method. In Section 3, numerical results are reported. Finally, in Section 4, we summarize our findings and discuss directions for future work.

II. THE MODEL AND ANALYTICAL CONSIDERATIONS

In what follows, we seek steady-state (standing-wave) solutions to system (1). We use the standing-wave ansatz,

$$\begin{cases} U(\vec{x},t) &= \sqrt{K}\, u(\vec{x})\, \exp[-iK(\mu - 2D\epsilon)\, t] \\ V(\vec{x},t) &= \sqrt{K}\, v(\vec{x})\, \exp[-iK(\mu - 2D\epsilon)\, t] \end{cases}, \tag{}$$

where $u(\vec{x})$ and $v(\vec{x})$ are real-valued functions, μ is the chemical potential (propagation constant) in the BEC (optics) model, shifted by the constant D; the latter takes the values $D = 1$ and 2 for the 1D and 2D cases, respectively. Substituting these expressions in Eqs. (1) leads to stationary equations, which, in the 1D model, take the form:

$$\begin{cases} \mu u_n = \epsilon \overline{\Delta}_1 u_n + v_n + u_n^3 \\ \mu v_n = \epsilon \overline{\Delta}_1 v_n + u_n + v_n^3 \end{cases}, \tag{2}$$

Where $\overline{\Delta}_1 w_n \equiv w_{n+1} + w_{n-1}$. In the 2D case, the stationary equations are:

$$\begin{cases} \mu u_{n,m} = \epsilon \overline{\Delta}_2 u_{n,m} + v_{n,m} + u_{n,m}^3 \\ \mu v_{n,m} = \epsilon \overline{\Delta}_2 v_{n,m} + u_{n,m} + v_{n,m}^3 \end{cases}, \tag{3}$$

Where $\overline{\Delta}_2 w_{n,m} \equiv w_{n+1,m} + w_{n-1,m} + w_{n,m+1} + w_{n,m-1}$.

Below, we aim to construct symmetric ($u = v$) and asymmetric ($u \neq v$) solutions of Eqs. (2) and (3). In order to develop an analytical approximation to the solutions, we resort to the variational method [23]. To this end, we notice that Eqs. (2) and (3) can be derived from the following Lagrangians:

$$L_{1D} = \sum_{n=-\infty}^{\infty} \left[-\frac{\mu}{2}\left(u_n^2 + v_n^2\right) + \frac{1}{4}\left(u_n^4 + v_n^4\right) + u_n v_n \epsilon \left(u_{n+1}u_n + v_{n+1}v_n\right) \right], \tag{4}$$

$$L_{2D} = \sum_{m,n=-\infty}^{\infty} \Big[-\frac{\mu}{2}\left(u_{n,m}^2 + v_{n,m}^2\right) + \frac{1}{4}\left(u_{n,m}^4 + v_{n,m}^4\right) + u_{n,m}^4 v_{n,m}^4 + \epsilon(u_{n+1,m}u_{n,m} + u_{n,m+1}u_{n,m} + v_{n+1,m}v_{n,m} + v_{n,m+1}v_{n,m}) \Big]. \tag{5}$$

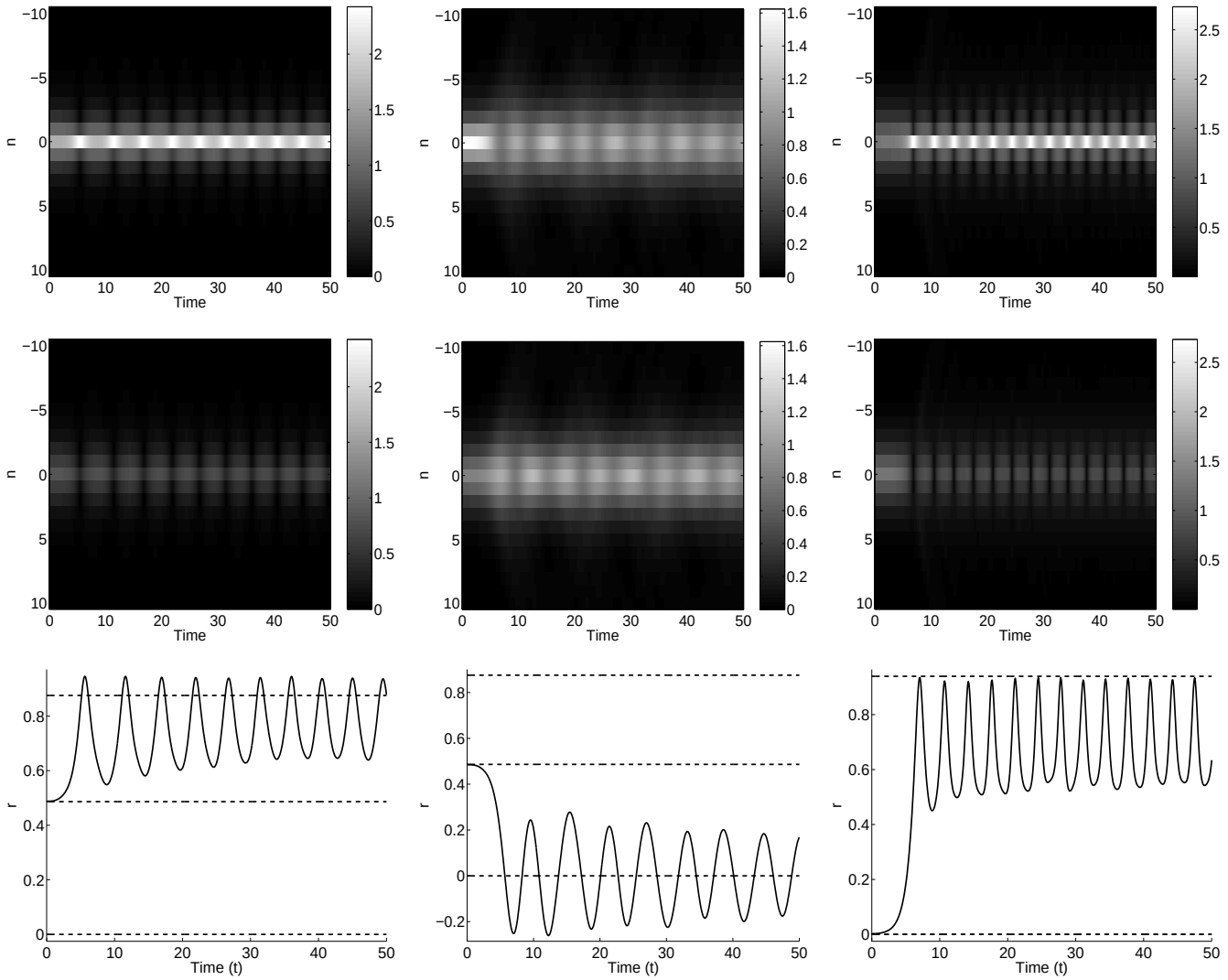

FIG. 5: Time-evolution plots for perturbed one-dimensional solutions from Fig. 2. The top (middle) row depicts the space-time contour plot evolution of $|U|^2$ ($|V|^2$). The first two columns are for two different perturbations of the solution shown in the second column of Fig. 4: the first column is generated by a perturbation which pushes the solution towards the upper stable asymmetric solution branch of the bifurcation diagram, while, in the second column, the perturbation pushes the solution towards the $r = 0$ solution. The last column is for a perturbation of the unstable symmetric solution (on the $r = 0$ curve) at $E = 4.1$, which pushes the solution towards the upper stable solution branch. The bottom row of figures displays the value of r as the solutions evolve in time, shown by the solid line, and the constant value of r for the steady states at the same energy level (dashed horizontal lines).

Further, we employ natural *ansätze*, $\{u_n, v_n\} = \{A, B\}e^{-\lambda|n|}$ and $\{u_{n,m}, v_{n,m}\} = \{A, B\}e^{-\lambda|n|}e^{-\lambda|m|}$, with free constants A, B and $\lambda > 0$, in the 1D and 2D cases, respectively. This choice is motivated both by the exponential decay of the solutions' tails far from the soliton's center and by the fact that only this type of the trial functions makes the approximation straightforwardly tractable [24]. Plugging the *ansätze* into Eqs. (4) and (5) and analytically evaluating the resulting geometric series, we arrive at the following expressions for the effective Lagrangians:

$$L_{1\mathrm{D}} = \left[AB - \frac{\mu}{2}\left(A^2 + B^2\right)\right]\coth\lambda + \frac{1}{4}\left(A^4 + B^4\right)\coth\left(2\lambda\right) + \epsilon\left(A^2 + B^2\right)\mathrm{cosech}\lambda \tag{6}$$

$$L_{2\mathrm{D}} = \left[AB - \frac{\mu}{2}\left(A^2 + B^2\right)\right]\coth^2\lambda + \frac{1}{4}\left(A^4 + B^4\right)\coth^2 2\lambda + 2\epsilon\left(A^2 + B^2\right)\left(\mathrm{cosech}\lambda\right)\coth\lambda. \tag{7}$$

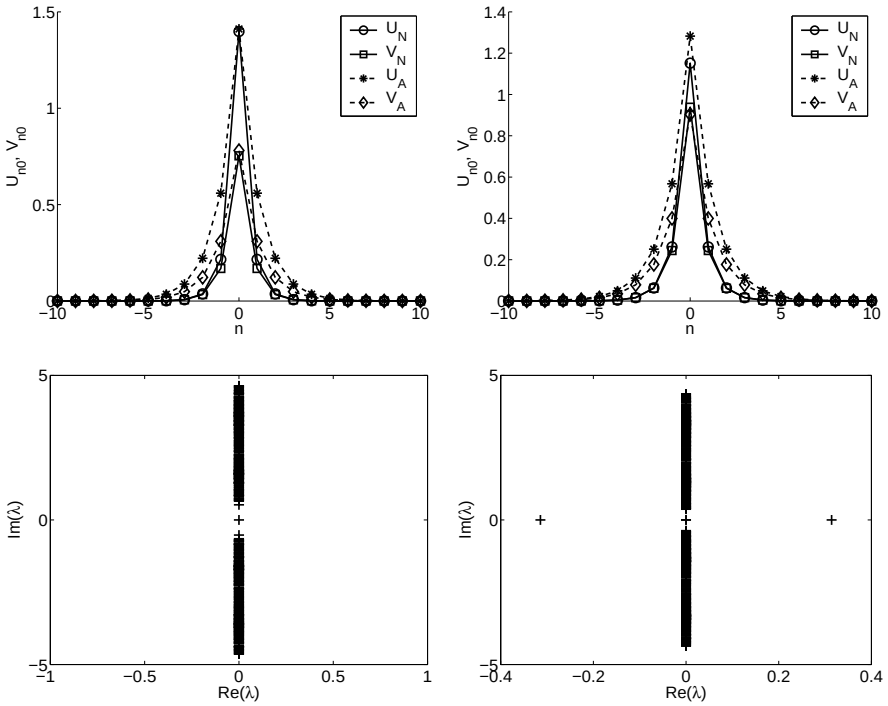

FIG. 6: Cross-section plots of the asymmetric solutions belonging to corresponding curve in Fig. 3, for $E = 1.435$. The top-row figures show the solutions found by means of the numerical (U_N, V_N) and variational ("analytical", U_A, V_A) methods, and the bottom row plots illustrate the stability eigenvalues for the numerical solution. As can be seen, the first and second columns represent, respectively, stable and unstable solutions belonging to the upper (outer) and inner curves (asymmetric branches) of the bifurcation diagram, respectively.

The static form of the Euler-Lagrange equations following from here, $\partial L_{1\mathrm{D},2\mathrm{D}}/\partial\left(\lambda, A, B\right) = 0$, is

$$\frac{\mu}{2}\left(A^2+B^2\right)\mathrm{cosech}^2\lambda - \frac{1}{2}\left(A^4+B^4\right)\mathrm{cosech}^2 2\lambda$$
$$-AB\mathrm{cosech}^2\lambda\epsilon\left(A^2+B^2\right)\mathrm{cosech}\lambda\coth\lambda = 0,$$

$$-\mu A\coth\lambda + A^3\coth 2\lambda + B\coth\lambda + 2\epsilon A\mathrm{cosech}\lambda = 0,$$

$$-\mu B\coth\lambda + B^3\coth 2\lambda + A\coth\lambda + 2\epsilon B\mathrm{cosech}\lambda = 0,$$

for the 1D case, and

$$\mu\left(A^2+B^2\right)\coth\lambda\mathrm{cosech}^2\lambda$$
$$-\left(A^4+B^4\right)\coth 2\lambda\mathrm{cosech}^2 2\lambda - 2AB\coth\lambda\mathrm{cosech}^2\lambda$$
$$-2\epsilon\left(A^2+B^2\right)\left(\mathrm{cosech}\lambda\coth^2\lambda + \mathrm{cosech}^3\lambda\right) = 0,$$

$$-\mu A\coth^2\lambda + A^3\coth^2 2\lambda + B\coth^2\lambda +$$
$$4\epsilon A\mathrm{cosech}\lambda\coth\lambda = 0,$$

$$-\mu B\coth^2\lambda + B^3\coth^2 2\lambda + A\coth^2\lambda$$
$$+4\epsilon B\mathrm{cosech}\lambda\coth\lambda = 0,$$

for the 2D case. These equations were solved for A, B, and λ and will be compared, in the next section, to the full numerical solution of Eqs. (2) and (3).

Another analytically tractable case corresponds to the anti-continuum limit of $\epsilon = 0$. For the symmetric branch, we then have $u_n = v_n = 0$ or $u_n = v_n = \sqrt{\mu - 1}$, while for the asymmetric branch, one needs to solve a system of algebraic equations, $\mu u_n = v_n + u_n^3$, $\mu + 1 = u_n^2 + u_n v_n + v_n^2$. The solution is shown in Fig. 1, which displays the respective symmetry-breaking bifurcation by means of a plot of the asymmetry measure, $r \equiv (E_1 - E_2)/(E_1 + E_2)$, versus half the total norm, $E = (E_1 + E_2)/2$, where $\{E_1, E_2\} = \sum_n \left\{u_n^2, v_n^2\right\}$ are the norms of the two components of the solution (in the BEC model, they are proportional to the number of atoms in the two atomic states, while in the optical setting they measure the total power of the beams in the two coupled lattices). As seen from the figure, the pitchfork bifurcation is supercritical in this limit (this will be compared to typical behavior for finite ϵ below).

III. NUMERICAL METHODS AND RESULTS

Numerical solutions to Eqs. (2) and (3) were found by using the method of the pseudo-arclength continuation [25, 26]. Another typical approach to solving systems of nonlinear equations for various values of a control parameter relies upon parameter continuation; however, this method fails for solution-parameter pairings where the

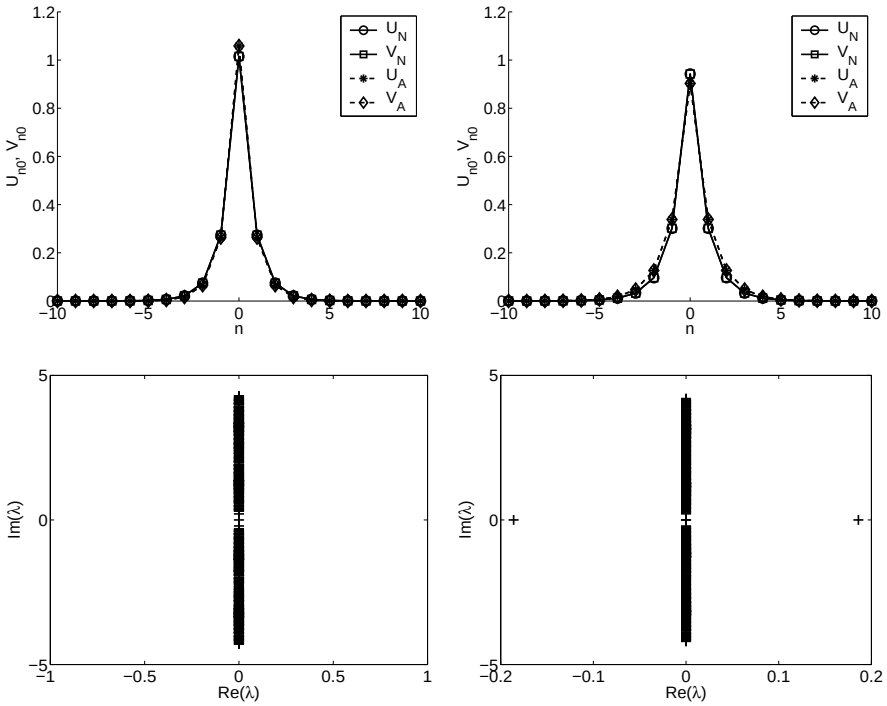

FIG. 7: Same as Fig. (6) for two symmetric solutions found at $E = 1.435$.

resulting Jacobian is singular. On the other hand, the pseudo-arclength continuation addresses this problem by introducing an extra pseudo-arclength parameter, and including an additional equation into the system, which makes the solution and control parameter dependent upon the pseudo-arclength. Calling the pseudo-arclength parameter s, the additional equation, $F(u, v, \mu, s) = 0$, must be chosen such that $F(\bar{u}, \bar{v}, \bar{\mu}, s = 0) = 0$, where $(\bar{u}, \bar{v}, \bar{\mu})$ is a solution of Eqs. (2) or (3). Thus, for F we used $F(u, v, \mu, s) = |u - \bar{u}|^2 + |v - \bar{v}|^2 + |\mu - \bar{\mu}|^2 - s^2$.

Once the steady states were identified, their stability was examined in the framework of linear stability analysis by substituting a perturbed solution, in the form of

$$\begin{cases} U(\vec{x}, t) &= e^{-i\mu t} \left[u(\vec{x}) + a(\vec{x})\, e^{\lambda t} + b^*(\vec{x})\, e^{\lambda^\star t} \right], \\ V(\vec{x}, t) &= e^{-i\mu t} \left[v(\vec{x}) + c(\vec{x})\, e^{\lambda t} + d^*(\vec{x})\, e^{\lambda^\star t} \right], \end{cases} \tag{8}$$

in Eqs. (1), the asterisk standing for complex conjugation. The linearized equations for the perturbation eigenmodes a, b, c, d were solved numerically, yielding eigenvalues λ associated with them.

The results are summarized in Figs. 2 and 3, for the 1D and 2D cases, respectively. In the 1D case, the symmetric branch, with $r = 0$, is stable for $E < 3.82$. Beyond this critical point, it becomes unstable through a *subcritical* pitchfork bifurcation, due to its collision with two unstable asymmetric branches. The VA predicts this critical point at $E \approx 3.92$, in good agreement with the numerical findings. Further, at another critical value, $E = 3.166$ (the corresponding VA prediction is $E \approx 3.128$) the unstable asymmetric branches turn back as stable ones, through a saddle-node bifurcation. Between the two critical points, both the symmetric branch and the outer asymmetric one are stable, hence there exists a region of bistability. To additionally demonstrate the accuracy of the VA, Fig. 4 presents comparison of the solution profiles at $E = 3.4$, together with the spectral plane, $(\mathrm{Re}(\lambda), \mathrm{Im}(\lambda))$, for the corresponding eigenvalues, $\lambda \equiv \mathrm{Re}(\lambda) + i\mathrm{Im}(\lambda)$. Recall that in Hamiltonian systems, such as the one considered here, if λ is an eigenvalue, so are also $-\lambda$, $\lambda^\star$ and $-\lambda^\star$, hence, if an eigenvalue with a nonzero real part exists, then the system will be linearly unstable.

For those 1D solutions that are linearly unstable due to a real eigenvalue, such as the unstable asymmetric solutions for $3.166 < E < 3.82$ and the symmetric ones for $E > 3.82$, we have examined their evolution in Fig. 5 by means of direct simulations of Eq. (1). In the case of the unstable asymmetric branch, the result of the evolution depends on the nature of the corresponding perturbation, due to the presence of the bistability in the corresponding parameter range: the solution ends up oscillating around either the stable asymmetric solution, or the stable symmetric one. The evolution of the unstable symmetric branch naturally results in oscillations around the stable asymmetric profile, which represents the ground state in that case.

An important observation in comparing Figs. 1 and 2 is that the bifurcation found in the anti-continuum limit shown in Fig. 1 is definitely supercritical, unlike the weakly subcritical one in Fig. 2. This indicates that the character of the bifurcation changes from subcritical to

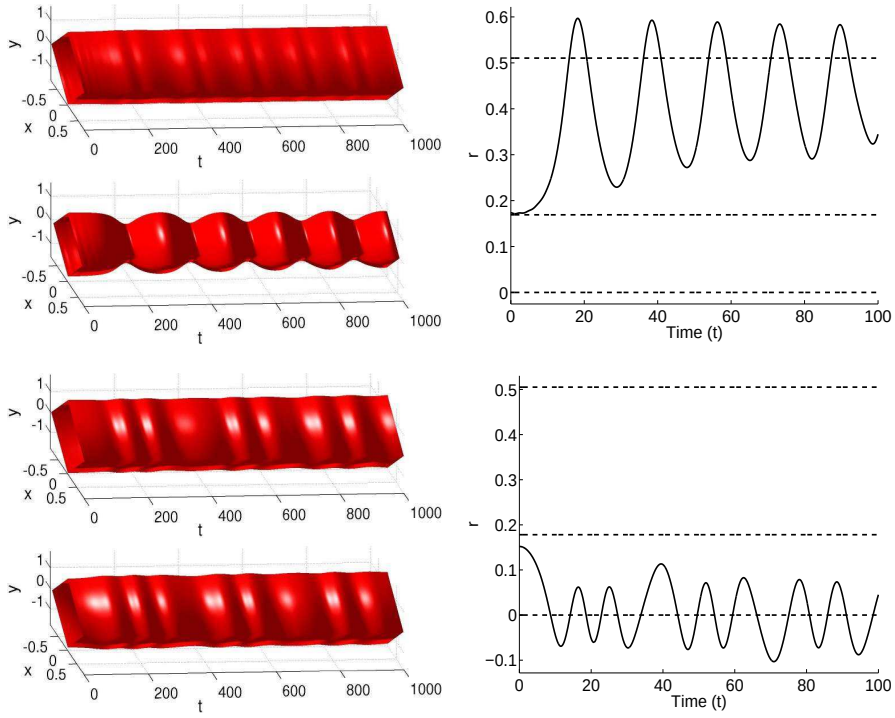

FIG. 8: Time-evolution plots for a perturbation of the unstable stationary state from Fig. 6. The top-row perturbation pushes the solution towards the upper stable part of the curve, while the bottom-row perturbation pushes it to the symmetric branch. The left column shows the three-dimensional space-time evolution of isodensity contours of the U (respective top subpanels) and V (respective bottom subpanels) solutions, while the right column shows the evolution of the asymmetry measure, r, from an unstable steady state towards a stable one (both are denoted by dashed lines).

supercritical pitchfork with the increase of discreteness, i.e., decrease of ϵ. This transition should eliminate the unstable asymmetric branches. In accordance with this expectation, we have found that the unstable asymmetric solutions exist only for $\epsilon > 0.35$, in the 1D case.

We now turn to the results for the 2D model collected in Fig. 3. Here, the results are even more interesting, for a number of reasons. On the one hand, there is no continuum analog to the bifurcation diagram, as the respective 2D continuum solutions are always unstable to collapse. Discreteness is well-known to arrest collapse [22, 27], generating branches of potentially stable localized solutions for sufficiently small values of the inter-site coupling constant (at a given chemical potential), or for sufficiently large chemical potential (at a given inter-site coupling), in one-component models [22]. Furthermore, in the 2D case, for a given value of the norm, there are two coexisting symmetric solutions, one (taller and narrower) with a larger chemical potential, which is stable, and one (shorter and wider) with a smaller chemical potential, which is unstable. As Fig. 3 implies, the symmetry-breaking weakly subcritical pitchfork bifurcation *typically* occurs from the stable branch of the symmetric solution, the corresponding critical point in Fig. 3 being $E \approx 1.45$. Similarly to the 1D case, there is also a saddle-node bifurcation between the unstable and stable asymmetric branches, which occurs at $E \approx 1.411$ and is responsible for the turning point.

In the 2D model too, the VA accurately captures the trends of the numerical results, even though the less accurate nature of the 2D ansatz prevents a quantitative matching of the resulting bifurcation diagrams. Detailed profiles of the numerical solutions and their VA-predicted counterparts are shown in Figs. 6 and 7, for the asymmetric and symmetric branches respectively, at $E = 1.435$. Two additional remarks are in order here. Firstly, similar to the 1D case, the 2D bifurcation changes character from weakly subcritical (as observed in Fig. 3) to supercritical (as seen in the anti-continuum limit of $\epsilon = 0$) at $\epsilon \approx 0.19$. On the other hand, as ϵ further increases, the stable part of the symmetric branch (in Fig. 3) shrinks and eventually disappears at $\epsilon > 0.29$.

Finally, we have again examined the dynamics of linearly unstable solutions, upon appropriate perturbations, through direct simulations, see Figs. 8 and 9. In the former figure, we have explored how the bistability, which is shown for a range of E in Fig. 3, "kicks" the unstable asymmetric solution either in the direction of its stable asymmetric counterpart, or towards the stable symmetric solution [it is relevant to stress here, in connection with Fig. 3, that, while the symmetric solution has a norm threshold at $E \approx 1.425$, the stable asymmetric solution can, in principle, be found at *lower* norms than the symmetric one, thus allowing the system to effectively de-

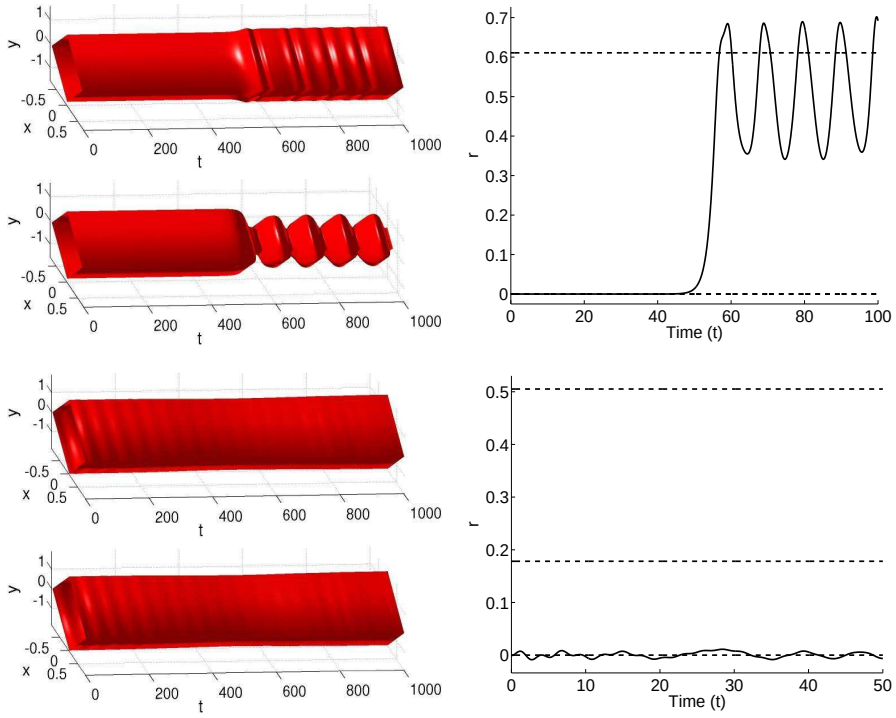

FIG. 9: Similar to the previous figure: the time-evolution plots for perturbations of two unstable symmetric steady states. The top row is for a solution with $E = 1.5$, and the bottom row is for the solution from Fig. 7. In the top row, the perturbation pushes the solution towards the upper asymmetric branch, while in bottom row the perturbation initiates the evolution of the solution towards the stable symmetric state.

crease its "excitation threshold" [28]]. In the latter figure, we consider the unstable symmetric branch, both when a stable symmetric branch does not exist, in which case the solution becomes asymmetric (top row), and when a stable symmetric branch does exist, in which case the system evolves towards that solution (bottom row).

IV. CONCLUSIONS

In this work, we have introduced the model based on two linearly coupled lattices with the cubic nonlinearity, and investigated its dynamical properties in detail. We have demonstrated that, in a number of respects, the discrete system emulates its continuum 1D counterpart, analyzed earlier in Refs. [16, 17, 18]. On the other hand, the lattice model gives rise to novel features. Even in the 1D setting, varying the strength of the lattice inter-site coupling may be used to switch the character of the bifurcation from subcritical to supercritical pitchfork, as the coupling gets weaker, and the anti-continuum limit is approached. In the more interesting 2D setting, our work is the first manifestation, to the best of our knowledge, of the existence of such a bifurcation diagram, since in the continuum limit the symmetry-breaking models with the self-focusing nonlinearity are irrelevant due to the collapse instability. Furthermore, the discreteness induces the presence of both stable and unstable branches of symmetric solutions, thus enriching the bifurcation diagram. In the 2D case, not only is it possible for weaker lattice coupling to turn the bifurcation from subcritical to supercritical, but it is also possible for the lattice (when the bifurcation is subcritical) to possess a lower excitation threshold for asymmetric states than for the symmetric ones. All of these features demonstrate critical modifications that the discreteness imposes on the well-known symmetry-breaking picture in continuum models.

It might be quite interesting to examine similar features in 3D and compare the results with their 2D and 1D counterparts. Of perhaps even more physical interest, especially in terms of coupled hyperfine states in BECs, would be to add nonlinear coupling between the lattice components, of the cross-phase-modulation type, to the linear coupling considered here. It would be particularly interesting to examine how the symmetry-breaking phenomenology is affected by the gradual increase of such a coupling. This study is currently in progress and the results will be reported elsewhere.

[1] S. Aubry, Physica D **103**, 201, (1997); S. Flach and C. R. Willis, Phys. Rep. **295** 181 (1998); D. Hennig and G. Tsironis, Phys. Rep. **307**, 333 (1999).

[2] P. G. Kevrekidis, K. Ø. Rasmussen, and A. R. Bishop, Int. J. Mod. Phys. B **15**, 2833 (2001).

[3] M. Sato, B. E. Hubbard, and A. J. Sievers Rev. Mod. Phys. **78**, 137 (2006).

[4] D. N. Christodoulides, F. Lederer and Y. Silberberg, Nature **424**, 817 (2003); Yu. S. Kivshar and G. P. Agrawal, *Optical Solitons: From Fibers to Photonic Crystals*, Academic Press (San Diego, 2003).

[5] V. V. Konotop and V. A. Brazhnyi, Mod. Phys. Lett. B **18** 627, (2004); O. Morsch and M. Oberthaler, Rev. Mod. Phys. **78**, 179 (2006); P. G. Kevrekidis and D. J. Frantzeskakis, Mod. Phys. Lett. B **18**, 173 (2004).

[6] M. Peyrard, Nonlinearity **17**, R1 (2004).

[7] J. Meier, J. Hudock, D. Christodoulides, G. Stegeman, Y. Silberberg, R. Morandotti, and J. S. Aitchison, Phys. Rev. Lett. **91**, 143907 (2003).

[8] J. Hudock, P. G. Kevrekidis, B. A. Malomed and D. N. Christodoulides, Phys. Rev. E **67**, 056618 (2003).

[9] C. J. Myatt, E. A. Burt, R. W. Ghrist, E. A˙Cornell, and C. E. Wieman Phys. Rev. Lett. **78**, 586 (1997).

[10] D. S. Hall, M. R. Matthews, J. R. Ensher, C. E. Wieman, and E. A. Cornell, Phys. Rev. Lett. **81**, 1539 (1998).

[11] D. M. Stamper-Kurn, M. R. Andrews, A. P. Chikkatur, S. Inouye, H.-J. Miesner, J. Stenger, and W. Ketterle, Phys. Rev. Lett. **80**, 2027 (1998).

[12] P. G. Kevrekidis, H. Susanto, R. Carretero-González, B. A. Malomed and D. J. Frantzeskakis, Phys. Rev. E **72**, 066604 (2005).

[13] B. A. Malomed and J. Yang, Phys. Lett. A **302**, 163 (2002).

[14] R. J. Ballagh, K. Burnett and T. F. Scott, Phys. Rev. Lett. **78**, 1607 (1997); B. Deconinck, P. G. Kevrekidis, H. E. Nistazakis, and D. J. Frantzeskakis, Phys. Rev. A **70**, 063605 (2004).

[15] P. Ohberg and S. Stenholm, Phys. Rev. A **59**, 3890 (1999); J. Williams, R. Walser, J. Cooper, E. Cornell and M. Holland, Phys. Rev. A **59**, R31 (1999).

[16] N. Akhmediev and J. M. Soto-Crespo, Phys. Rev. E **49**, 4519 (1994).

[17] B. A. Malomed, I. M. Skinner, P. L. Chu and G. D. Peng, Phys. Rev. E **53**, 4084 (1996).

[18] W.C.K. Mak, B. A. Malomed, and P. L. Chu, Phys. Rev. E **55**, 6134 (1997); **57**, 1092 (1998); J. Opt. Soc. Am. B **15**, 1685 (1998); L. Albuch and B. A. Malomed, Math. Comp. Simul. **74**, 312 (2007).

[19] A. Locatelli, D. Modotto, D. Paloschi and C. De Angelis, Opt. Comm. **237**, 97 (2004).

[20] S. Inouye, M. R. Andrews, J. Stenger, H.-J. Miesner, D. M. Stamper-Kurn, and W. Ketterle, Nature **392**, 151 (1998);
J. Stenger, S. Inouye, M. R. Andrews, H.-J. Miesner, D. M. Stamper-Kurn, and W. Ketterle, Phys. Rev. Lett. **82**, 2422 (1999);
J. L. Roberts, N. R. Claussen, J.P. Burke, Jr., C. H. Greene, E. A. Cornell, and C. E. Wieman, Phys. Rev. Lett. **81**, 5109 (1998);
S. L. Cornish, N. R. Claussen, J. L. Roberts, E. A. Cornell, and C. E. Wieman Phys. Rev. Lett. **85**, 1795 (2000);
E. A. Donley, N. R. Claussen, S. L. Cornish, J. L. Roberts, E. A. Cornell, and C. E. Wieman, Nature **412**, 295 (2001).

[21] C. Sulem and P. L. Sulem, *The Nonlinear Schrödinger Equation*, Springer-Verlag (New York, 1999).

[22] P. G. Kevrekidis, K. Ø. Rasmussen, and A. R. Bishop Phys. Rev. E **61**, 2006 (2000).

[23] B. A. Malomed, in *Progress in Optics*, vol. 43, p. 71 (ed. by E. Wolf; North-Holland: Amsterdam, 2002).

[24] B. A. Malomed and M. I. Weinstein, Phys. Lett. A **220**, 91 (1996).

[25] E. L. Allgower and K. Georg, *Numerical Path Following*. In P. G. Ciarlet and J. L. Lions, *Handbook of Numerical Analysis, Volume 5* 3-207 (North-Holland (1997)).

[26] H. B. Keller, *Numerical Solution of Bifurcation and Nonlinear Eigenvalue Problems*. In P. H. Rabinowitz, *Applications of Bifurcation Theory* 359-384 (Academic Press, New York, 1977).

[27] G. Fibich, B. Ilan, Appl. Numer. Math. **44**, 63 (2003); N. Tzirakis and P. G. Kevrekidis, Math. Comp. Simul. **69**, 553 (2004).

[28] S. Flach, K. Kladko and R. S. MacKay, Phys. Rev. Lett. **78**, 1207 (1997); M. Weinstein, Nonlinearity **12**, 673 (1999).